Electronic Supplementary Material (ESI) for Inorganic Chemistry Frontiers.

Efficient electrocatalytic nitrogen oxidation to nitrate over the self-assembly of supramolecular cucurbit[6]uril with heteropolyacid

Manli Xu[a], Xianyan Ao[a], Chengcheng Son[b],Liling Zeng[a], Chao Zhang[a], Yunqian Zhang*[a], Wenfen Zhao*[b]

[a] Key Laboratory of Macrocyclic and Supramolecular Chemistry of Guizhou Province, Guizhou University, Guiyang 550025, People's Republic of China

[b] School of Chemistry and Chemical Engineering, Guizhou University, Guiyang 550025, China

Corresponding Author: E-mail: sci.yqzhang@gzu.edu.cn, zhaowf@gzu.edu.cn

Experimental

5% Nafion, phosphomolybdic acid (PMA), Na_2SO_4, Graphitic carbon, isopropanol (C_3H_8O), H_2SO_4, and NaOH were purchased from Aladdin Bio-Chem Technology Co., LTD (Shanghai, China). And were used without purification. Pure water was used for all experiments. The Cucurbit[6]uril (Q[6]) was prepared according to reference.[1] Ar (≥ 99.999%), and N_2 (≥ 99.999%) were purchased from Guizhou Sanhe Yongxin Trading Co., LTD.

Preparation of Q[6]-PMA

Dissolved 50 mg of Q[6] in 50 mL of 3 M HCl solution. PMA was weighed in a molar ratio of 1:1 concerning Q[6], and dissolved in 50 mL of pure water. The PMA solution was added to the Q[6] solution at room temperature using a constant pressure funnel with a controlled drop rate of 10 drops per minute. A green precipitate was obtained, washed with pure water, and dried in a vacuum at 40 ℃ to obtain Q[6]-PMA with a yield of 86.7%.

Potassium phosphomolybdate (PMK): Under ambient conditions, 100 mL of 0.21 M KCl aqueous solution was added drop wise into 0.034 M 200 mL of PMA aqueous solution to obtain a yellow precipitate, which was washed with pure water and dried at 80 ℃.

Characterization

The XPS data was obtained via Thermo Scientific ESCALAB Xi. SEM (JSM-7610FPlus), TEM (HT7800), and EDX were used to analyze the morphology of the samples. Raman tests were performed at 785 nm, FTIR (BRUKER Alpha) in the range 400 cm^{-1}– 4000 cm^{-1}, and the XRD data were collected at Ultima IV (Cu Ka 1.54 A). Thermogravimetric Differential Scanning Calorimetry (TG-DSC) was tested using STA2500 in the N_2 atmosphere. Nitrogen adsorption and desorption isotherms were tested using ASAP 2460 at 77 K (samples were prepared using vacuum degassing at 110°C for 6 hours before testing). EA (Elementar vario EL cube) was used to determine the organic element content. ICP-OES (ICAP-7000) was tested for P and Mo. Nitrate absorbance was tested using UV-2700. Standard NO_3^- and NO_2^- infrared data were tested by ATR-FTIR (IRTracer 100).

Electrochemical measurement

Electrochemical measurements were performed using CHI 760E electrochemical analyzer (CH Instruments, Inc., Shanghai). A leak-free Ag/AgCl, platinum sheet, and glassy carbon electrodes (GCE) were used as reference, auxiliary, and working electrodes, respectively. Hermetically sealed single-chamber electrolytic cells were used as electrolytic cells. All electrochemical tests were carried out in pH 6.8 0.1 M Na_2SO_4 solution at ambient conditions, and the working potentials were converted to reversible hydrogen electrodes (RHEs) in data processing.

$$\mathbf{E_{(vs.RHE)} = E_{(Ag/AgCl)} + 0.197 + 0.059 \times pH} \quad (1)$$

Modified electrode preparation: 2.5 mg of Q[6]-PMA was added to 200 μL of pure

water, 200 μL of isopropanol, 20 μL of Nafion, 1.0 mg of graphitic carbon, sonicated for half an hour, and 3.0 μL drops were taken to the GCE.
Add 20 mL of 0.1 M Na_2SO_4 solution to a sealed electrolytic cell. The N_2 flow rate was 15 mL min^{-1} and was purified with 0.05 M H_2SO_4 before entering a sealed electrolytic cell.

Determination of nitrate

The concentration-absorbance curve was calibrated with a series of standard potassium nitrate solutions, and a concentration-peak area standard curve was established using ion chromatography (ICS-1100).
Take 5 mL of electrolyte solution and add 0.1 mL of 1M HCl and 0.01 mL of 0.8 wt % sulfanilic acid solution. The absorption spectra were measured with UV–vis, and the absorption intensities at 220 nm and 275 nm wavelengths were recorded. The calculation formula for final absorbance:

$$\mathbf{A = A_{220nm} - 2A_{275nm}} \quad (2)$$

Nitrate yield

$$\mathbf{R_{NO_3^-} = \frac{C_{NO_3^-} \times V}{t \times m_{cat}}} \quad (3)$$

Nitrate Faraday efficiency

$$\mathbf{FE = \frac{5 \times F \times C_{NO_3^-} \times V}{Q}} \quad (4)$$

R is the yield of NO_3^-, C is the measured NO_3^- concentration (μg mL^{-1}), V is the total volume of electrolyte (mL), it is the time of electrocatalysis (h), and mcat is the weight of loaded catalyst (mg). F is the Faraday constant, and Q is the total charge through the working electrode.

TOF calculation method

$$\mathrm{TOF} = \frac{\text{The converted amount of nitrogen}}{\text{Number of active sites} \times \text{Time}}$$

The converted amount of nitrogen is approximate to molar amount of NO_3^- (mol); the number of active sites was calculated by the Mo content in ICP; time is the CA test time (h).

In situ FTIR testing

Prior to testing, the purified N_2 was passed continuously for 30 min into a Spectroelectrochemical cell containing 0.1 M Na_2SO_4 solution at a flow rate of 15 mL min^{-1}. Then, a background spectrum was collected and used for the 2.2 V vs. RHE CA test. Simultaneously, in situ, ATR-FTIR measurements were synchronously triggered at a resolution of 4 $cm^{-1,}$ and the corresponding spectra were recorded by the software. In situ electrochemical FTIR under argon condition is carried out under the same conditions.

Isotopic labeling experiments

Isotopic labeling electrochemical NOR experiments were performed using $^{15}N_2$ as raw material to instead of standard $^{14}N_2$. Before conducting the electrochemical test, the electrolyte was purged with $^{15}N_2$ for 10 min, and then the NOR test was performed at 2.2 V vs. RHE for 4 h. Subsequently, the electrolyte was concentrated to 2 mL and then analyzed via isotope-ratio mass spectrometry (Delta V Advantage).

Quantum chemical computing

All calculations were done in the Gaussian 09.[2] Constructed initial geometries of supramolecular complexes based on X–ray crystal structures,[3] according to density functional theory M06L theoretical method. The metal Mo atom used the LANL2DZ group, and all-electron 6-311G (d,p) groups were used for the other atoms. Boys and Bernardi functions were used to correct the binding energy of supramolecular interactions using basis set superposition error (BSSE).

Supplementary Figures

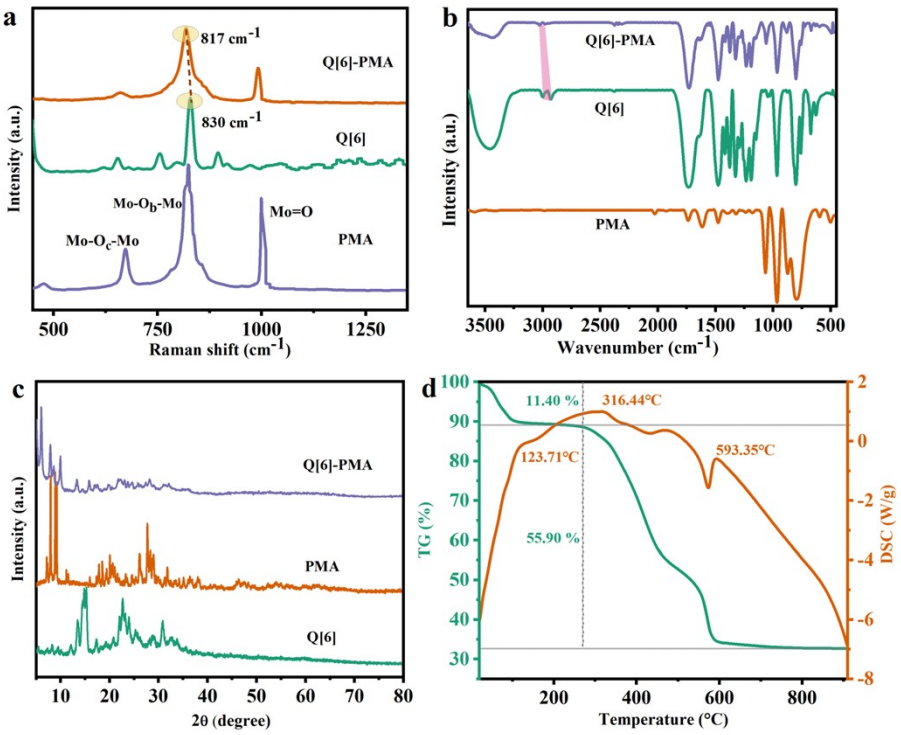

Fig. S1 Characterization of Q[6]-PMA (a) Raman, (b) FTIR, (c) XRD, and (d) TG-DSC.

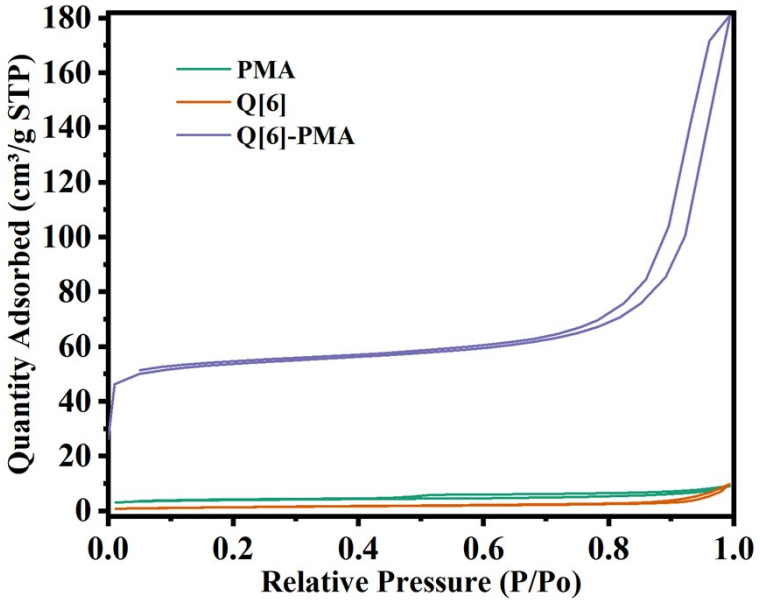

Fig. S2 N_2 adsorption and desorption curve of Q[6]-PMA.

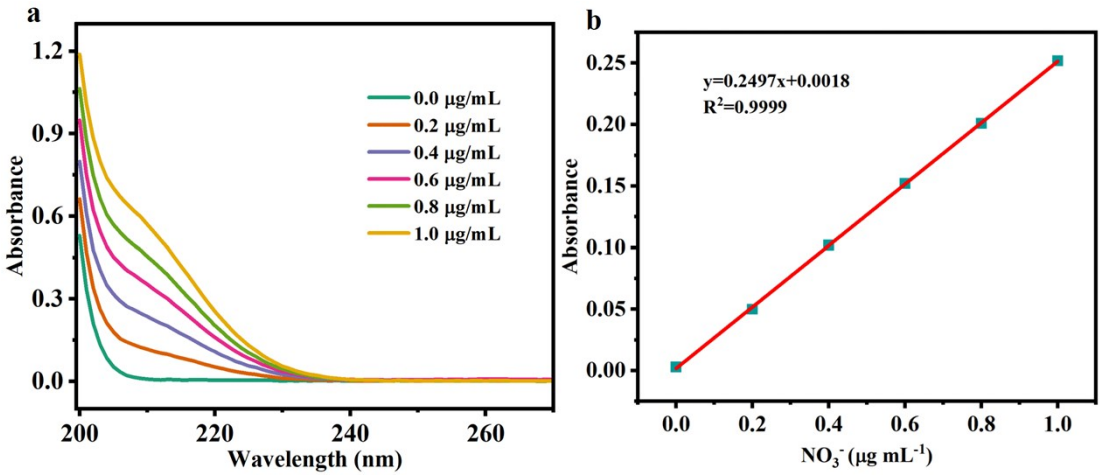

Fig. S3 (a)Standard NO_3^- UV–vis spectrum, (b) NO_3^- calibration curve.

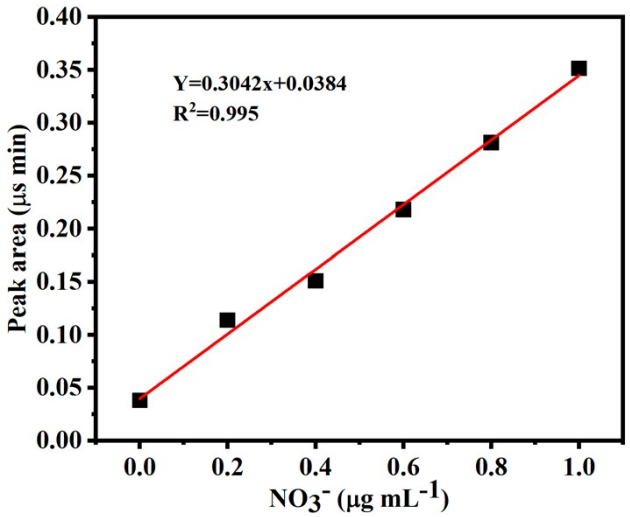

Fig. S4 Calibration curves for NO_3^- ion chromatography (IC).

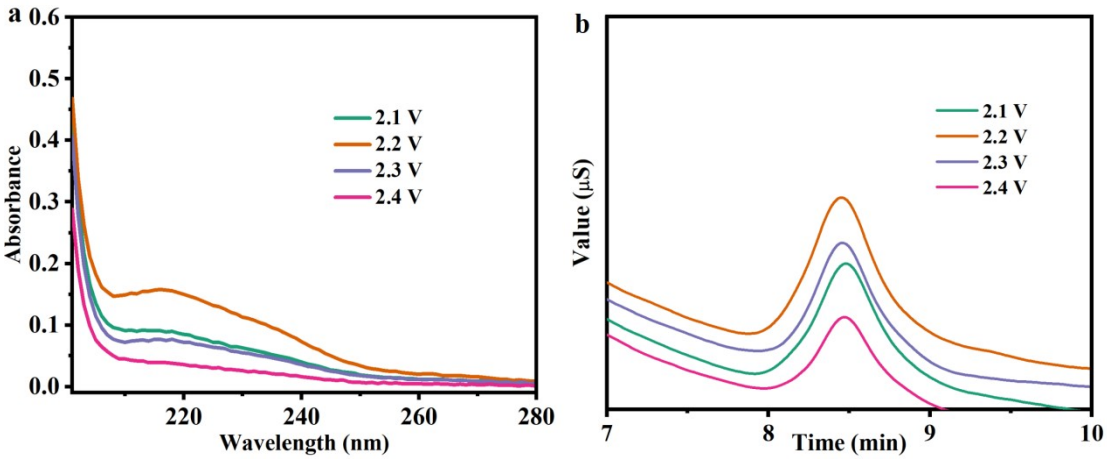

Fig. S5 NO_3^- detection of Q[6]-PMA electrocatalytic NOR at different potentials: (a) Uv–vis and (b) IC.

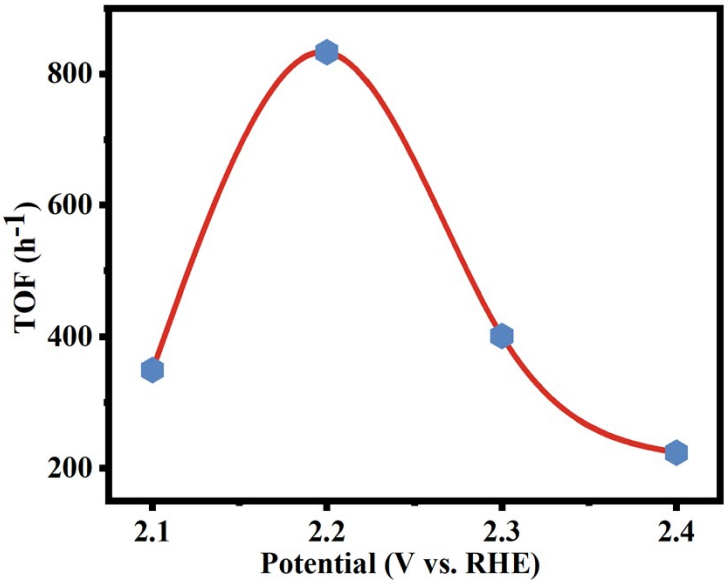

Fig. S6 TOF values of Q[6]-PMA in 0.1 M Na_2SO_4 solution at different potentials.

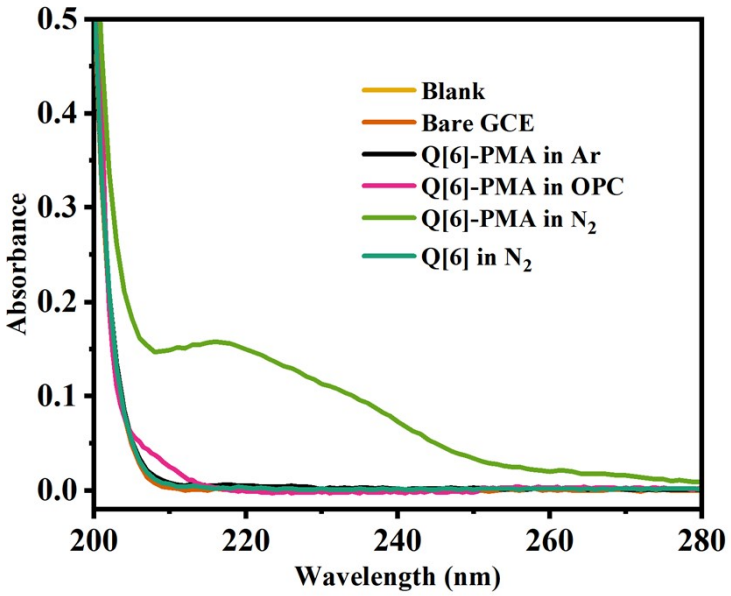

Fig. S7 Uv–vis spectra of blank electrolyte, Q[6] and Q[6]-PMA at N_2 saturated electrolyte, and Q[6]-PMA at Ar saturated electrolyte conditions at an open circuit voltage of 2.2 V vs. RHE.

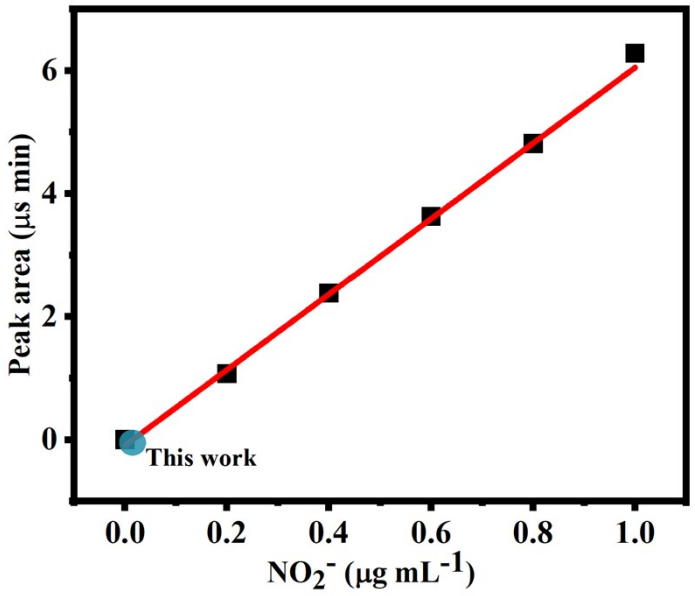

Fig. S8 Calibration curves for NO_2^- ion chromatography (IC).

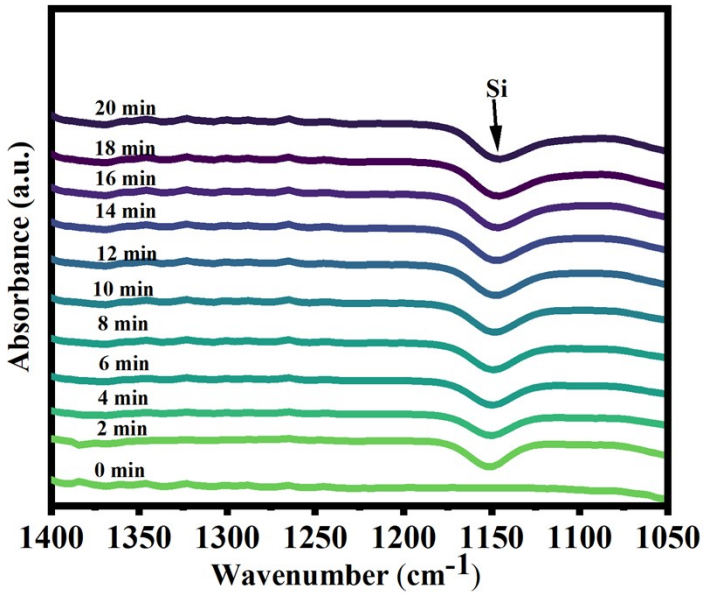

Fig. S9 Electrochemistry in situ FTIR of Q[6]-PMA under argon.

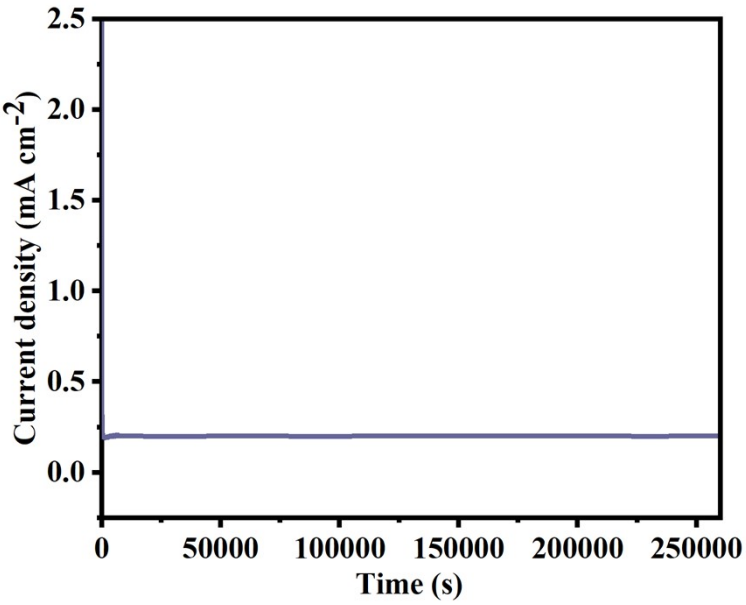

Fig. S10 Q[6]-PMA electrocatalytic NOR performance, 72-hour CA test at 2.2 V vs. RHE.

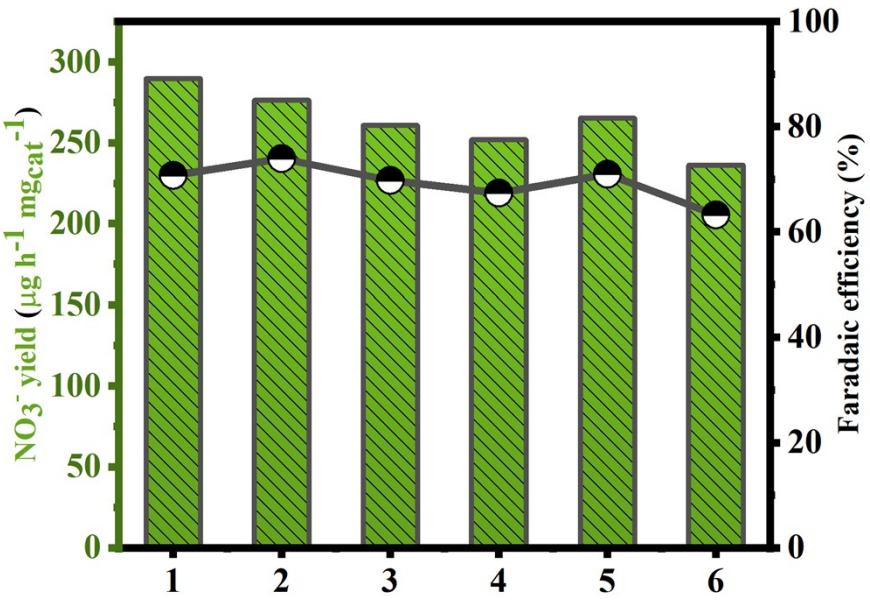

Fig. S11 NO_3^- yield and FE in 6 cycles of Q[6]-PMA electrocatalytic NOR.

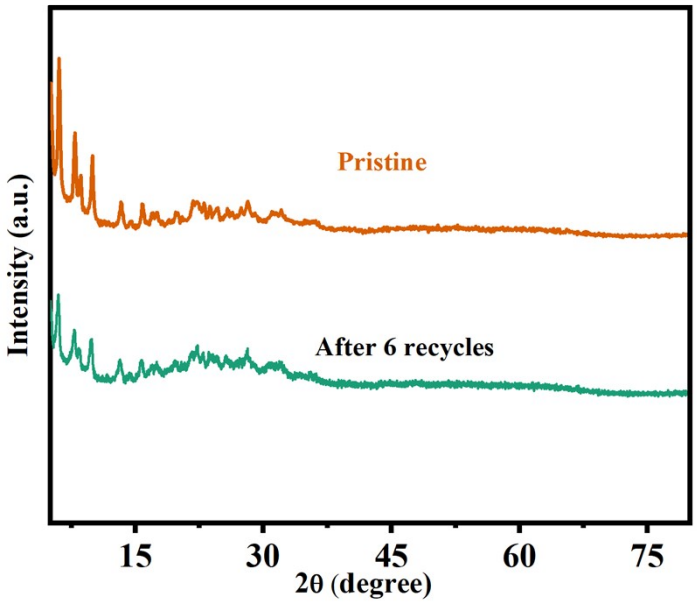

Fig. S12 XRD patterns of Q[6]-PMA pristine, after 6 recycles.

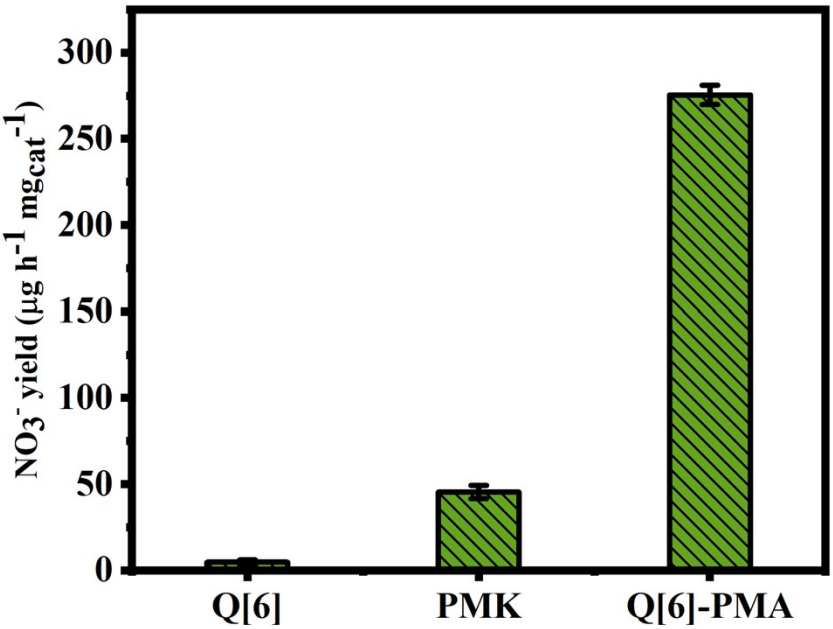

Fig. S13 NO_3^- yield of Q[6], PMK, and Q[6]-PMA at 2.2 V vs. RHE.

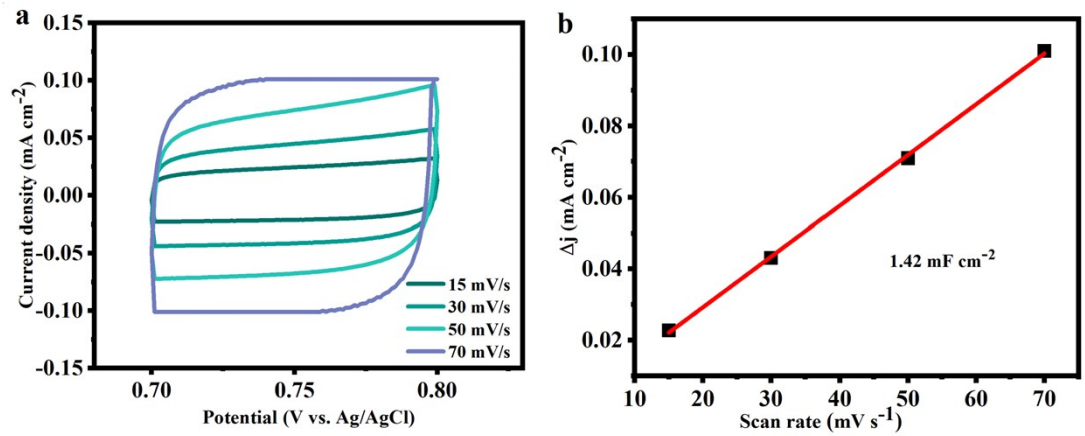

Fig. S14 (a) CV of Q[6]-PMA at different scanning speeds, (b) the function between current density and scanning rate in the CV curve.

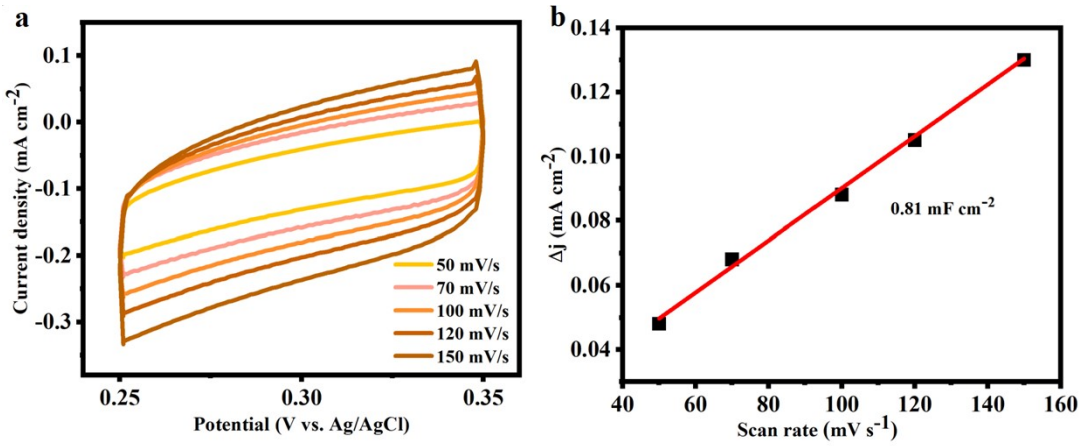

Fig. S15 (a) CV of Q[6] at different scanning speeds, (b) the function between current density and scanning rate in the CV curve.

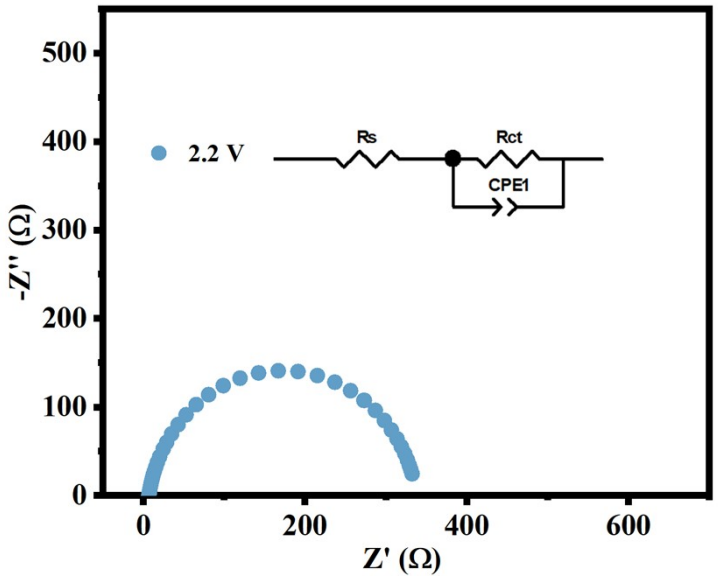

Fig. S16 In N_2 saturation of 0.1 M Na_2SO_4 solution, Q[6]-PMA under 2.2 V vs. RHE of NOR of impedance spectroscopy.

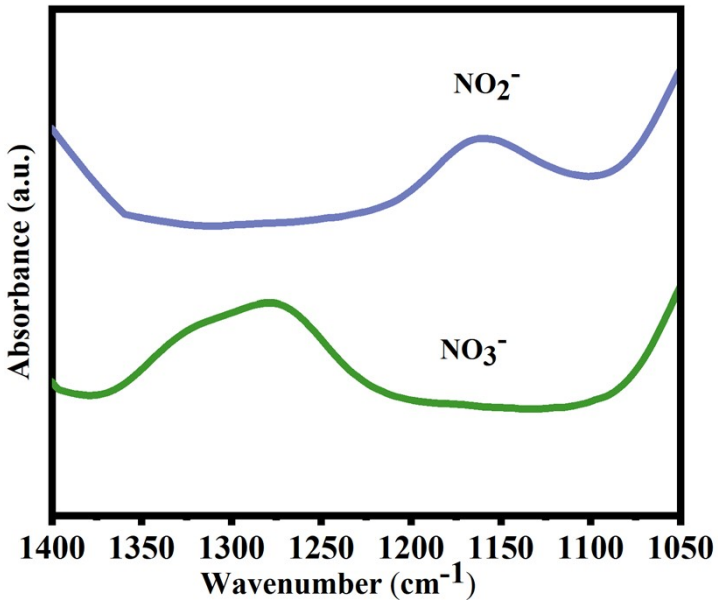

Fig. S17 Spectra of standard NO_3^- and NO_2^- detected by ATR-IR in 0.1M Na_2SO_4 solution.

Table S1. EA and ICP determination of Q [6]-PMA Element Content.

EA		ICP	
C%	18.821%	Mo%	20.47%
N%	14.615%	P%	0.72%
O%	35.605%		

Table S2. Q[6], PMA, and Q[6]-PMA nitrogen adsorption–desorption isotherm.

Electrode Material	BET Surface Area	micropore volume	pore size
Q[6]	5.2066 m^2/g	0.000683 cm^3/g	13.6043 nm
PMA	14.0674 m^2/g	0.004626 cm^3/g	6.6465 nm
Q[6]-PMA	**167.1707 m^2/g**	**0.066453 cm^3/g**	**20.5522 nm**

Table S3. Optimal NO_3^- yield and Faradaic efficiency (FE) of different electrolytes under ambient conditions.

Catalyst	electrolyte	Potential (V vs. RHE)	NO_3^- yield rate	FE(%)	Ref.
Q[6]-PMA	0.1 M Na_2SO_4	2.2	276.33 μg h^{-1} mg_{cat}^{-1}	73.93	Our work
PCN-222(Fe)	0.1 M HCl	1.6	110.9 μg h^{-1} mg_{cat}^{-1}	70.7	4
5MTO@FTO	0.1 M K_2SO_4	2.1	5.83 μg h^{-1} mg_{cat}^{-1}	~7	5
Fe-SnO_2	0.05 M H_2SO_4	1.96	42.9 μg h^{-1} mg_{cat}^{-1}	0.84	6
Au-Nb_2O_{5-x}	0.1 M Na_2SO_4	2.4	2.29 μg h^{-1} mg_{cat}^{-1}	2.06	7
2.79Ru/TiO_2	0.1 M Na_2SO_4	1.8	161.9 μg h^{-1} mg_{cat}^{-1}	26.1	8

Pd-s PNSs	0.1 M KOH	1.75	18.56 μg h^{-1} mg_{cat}^{-1}	~1.1	9
Pd-MXene	0.01 M Na_2SO_4	/	2.80 μg h^{-1} mg_{cat}^{-1}	11.34	10
Mo-O-C	0.1 M Na_2SO_4	2.35	217.1 μg h^{-1} mg_{cat}^{-1}	7.8	11
Ru-Mn_3O_4	0.1 M Na_2SO_4	1.6	23.28 μg h^{-1} mg_{cat}^{-1}	28.87	12
Pt	0.3 M K_2SO_4	2.19	0.060 μ mol h^{-1} cm^{-2}	1.23	13
$Pd_{0.9}Ru_{0.1}$	0.1 M KOH	1.7	0.078 μg h^{-1} mg_{cat}^{-1}	0.61	14
Ru NPs	0.1 M KOH + 0.5 M SO_4^{2-}	1.9	10.42 μg h^{-1} mg_{cat}^{-1}	/	15
$ZnFe_{0.4}Co_{1.6}O_4$	1 M KOH	1.5	49.8 μg h^{-1} g_{Mo}^{-1}	10.1	16
AD-Fe NS	0.05 M K_2SO_4	2.1	2.45 μ mol h^{-1} cm^{-2}	35.63	17
Fe-TiO_2/PE	methanol-water	3.5	7055.81 μmol h^{-1} g^{-1}_{cat}	~10	18
$B_{13}C_2$	0.1 M Na_2SO_4	2.4	165.8 μg h^{-1} mg_{cat}^{-1}	~5	19
L-V_2O_5NDs	0.1 M Na_2SO_4 (pH=10.5)	2.4	1388.0 μg h^{-1} mg_{cat}^{-1}	~1	20

References

1 R. Behrend, E. Meyer, F. Rusche, Condensation products from glycoluril and fromaldehyde. *Justus Liebigs Ann. Chem.*, 1905, **339**, 1-37.

2 M.-J. Frisch, G-W. Trucks, H.-B. Schlegel, G.-E. Scuseria, M.-A. Robb, J.-R. Cheeseman, G. Scalmani, V. Barone, B. Mennucci, G.-A. Petersson, H. Nakatsuji, M. Caricato, X. Li, H.-P. Hratchian, A. F. Izmaylov, J. Bloino, G. Zheng, J.-L. Sonnenberg, M. Hada, M. Ehara, K. Toyota, R. Fukuda, J. Hasegawa, M. Ishida, T. Nakajima, Y. Honda, O. Kitao, H. Nakai, T. Vreven, J.-A. Montgomery, J. E. Jr. Peralta, F. Ogliaro, M. Bearpark, J.-J. Heyd, E. Brothers, K. N. Kudin, V. N. Staroverov, R. Kobayashi, J. Normand, K. Raghavachari, A. Rendell, J. C. Burant, S. S. Iyengar, J. Tomasi, M. Cossi, N. Rega, J. M. Millam, M. Klene, J.-E. Knox, J. B.Cross, V. Bakken, C. Adamo, J. Jaramillo, R. Gomperts, R. E. Stratmann, O. Yazyev, A.-J. Austin, R. Cammi, C. Pomelli, J. W. Ochterski, R. L. Martin, K. Morokuma, V. G. Zakrzewski, G.-A. Voth, P. Salvador, J.-J. Dannenberg, S. Dapprich, A.-D. Daniels, O. Farkas, J.-B.Foresman, J.-V. Ortiz, J. Cioslowski, D.-J. Fox, *Gaussian, Inc.*: Wallingford CT, 2009.

3 X.-Y. Jin, J. Zhao, Q.-M. Ge, N. Jiang, M. Liu, H. Cong, Y.-Q. Zhang, Carbon nanomaterials made from supramolecular hybridization of cucurbit[6]uril with phosphomolybdic acid for supercapacitors. *ACS Appl. Nano Mater.*, 2023, **6**, 2459-2471.

4 H. He, H.-K. Li, Q.-Q. Zhu, C.-P. Li, Z. Zhang and M. Du, Hydrophobicity modulation on a ferriporphyrin-based metal-organic framework for enhanced ambient electrocatalytic nitrogen fixation, *Appl. Catal. B Environ.*, 2022, **316**, 121673.

5 M. Yu, G. Fan, J. Liu, W. Xu, J. Li and F. Cheng, Self-supported Mo-doped TiO_2 electrode for ambient electrocatalytic nitrogen oxidation, *Electrochimica Acta*, 2022, **435**, 141333.

6 L. Zhang, M. Cong, X. Ding, Y. Jin, F. Xu, Y. Wang, L. Chen and L. Zhang, A Janus Fe-SnO_2 catalyst that enables bifunctional electrochemical nitrogen fixation, *Angew. Chem. Int. Ed.*, 2020, **59**, 10888-10893.

7 Y. Zhang, F. Du, R. Wang, X. Ling, X. Wang, Q. Shen, Y. Xiong, T. Li, Y. Zhou and Z. Zou, Electrocatalytic fixation of N_2 into NO_3^-: electron transfer between oxygen vacancies and loaded Au in Nb_2O_{5-x} nanobelts to promote ambient nitrogen oxidation, *J. Mater. Chem. A*,

2021, **9**, 17442-17450.

8 M. Kuang, Y. Wang, W. Fang, H. Tan, M. Chen, J. Yao, C. Liu, J. Xu, K. Zhou and Q. Yan, Efficient nitrate synthesis via ambient nitrogen oxidation with Ru-Doped TiO_2/ RuO_2 electrocatalysts, *Adv. Mater.*, 2020, **32**, 2002189.

9 S. Han, C. Wang, Y. Wang, Y. Yu and B. Zhang, Electrosynthesis of nitrate via the oxidation of nitrogen on Tensile-Strained Palladium porous nanosheets, *Angew. Chem. Int. Ed.*, 2021, **60**, 4474-4478.

10 W. Fang, C. Du, M. Kuang, M. Chen, W. Huang, H. Ren, J. Xu, A. Feldhoff and Q. Yan, Boosting efficient ambient nitrogen oxidation by a well-dispersed Pd on MXene electrocatalyst, *Chem. Commun.*, 2020, **56**, 5779-5782.

11 S. Zhang, T. Shi, K. Li, Q. Sun, Y. Lin, L. R. Zheng, G. Wang, Y. Zhang, H. Yin and H. Zhang, Ambient electrochemical nitrogen fixation over a bifunctional Mo–$(O–C_2)_4$ site catalyst, *J. Phys. Chem. C*, 2022, **126**, 965-973.

12 Z. Nie, L. Zhang, X. Ding, M. Cong, F. Xu, L. Ma, M. Guo, M. Li and L. Zhang, Catalytic kinetics regulation for enhanced electrochemical nitrogen oxidation by Ru-Nanoclusters-Coupled Mn_3O_4 catalysts decorated with atomically dispersed Ru atoms, *Adv. Mater.*, 2022, **34**, 2108180.

13 Y. Wang, Y. Yu, R. Jia, C. Zhang and B. Zhang, Electrochemical synthesis of nitric acid from air and ammonia through waste utilization, *Nat. Sci. Rev.*, 2019, **6**, 730-738.

14 T. Li, S. Han, C. Wang, Y. Huang, Y. Wang, Y. Yu and B. Zhang, Ru-Doped Pd nanoparticles for nitrogen electrooxidation to nitrate, *ACS Catal*., 2021, **11**, 14032-14037.

15 T. Li, S. Han, C. Cheng, Y. Wang, X. Du, Y. Yu and B. Zhang, Sulfate-Enabled nitrate synthesis from nitrogen electrooxidation on a Rhodium electrocatalyst, *Angew. Chem. Int. Ed.*, 2022, **61**, e202204541.

16 C. Dai, Y. Sun, G. Chen, A. C. Fisher and Z. J. Xu, Electrochemical oxidation of nitrogen towards direct nitrate production on spinel oxides, *Angew. Chem., Int. Ed.*, 2020, **59**, 9418-9422.

17 Y. Guo, S. Zhang, R. Zhang, D. Wang, D. Zhu, X. Wang, D. Xiao, N. Li, Y. Zhao, Z. Huang, W. Xu, S. Chen, L. Song, J. Fan, Q. Chen and C. Zhi, Electrochemical nitrate production via nitrogen oxidation with atomically dispersed Fe on N-Doped carbon nanosheets, *ACS Nano*, 2021, **16**, 655-663.

18 M. Guo, L. Fang, L. Zhang, M. Li, M. Cong, X. Guan, C. Shi, C. Gu, X. Liu, Y. Wang and X. Ding, Pulsed electrocatalysis enabling high overall nitrogen fixation performance for atomically dispersed Fe on TiO_2, *Angew. Chem. Int. Ed*., 2023, **62**, e202217635.

19 J. Lan, M. Luo, J. Han, M. Peng, H. Duan and Y. Tan, Nanoporous $B_{13}C_2$ towards highly efficient electrochemical nitrogen fixation, *Small*, 2021, **17**, 2102814.

20 W. Li, Y. Ye, M. Jin, S. Zhang, C. Lin, C. Sun, Y. Zhang, G. Wang, C. Liang and H. Zhang, Ambient electrochemical nitrogen fixation with aqueous V_2O_5 nanodots in a fluidized electrocatalysis system, *Chem. Eng. J.*, 2023, **452**, 139494.